HAL open science

An implicit-explicit finite volume scheme for the fully nonlinear Serre system of equations

Denys Dutykh, Didier Clamond, Paul Milewski, Dimitrios Mitsotakis

▶ **To cite this version:**

Denys Dutykh, Didier Clamond, Paul Milewski, Dimitrios Mitsotakis. An implicit-explicit finite volume scheme for the fully nonlinear Serre system of equations. 2011. hal-00587994v1

HAL Id: hal-00587994

https://hal.science/hal-00587994v1

Preprint submitted on 22 Apr 2011 (v1), last revised 12 Feb 2013 (v4)

HAL is a multi-disciplinary open access archive for the deposit and dissemination of scientific research documents, whether they are published or not. The documents may come from teaching and research institutions in France or abroad, or from public or private research centers.

L'archive ouverte pluridisciplinaire **HAL**, est destinée au dépôt et à la diffusion de documents scientifiques de niveau recherche, publiés ou non, émanant des établissements d'enseignement et de recherche français ou étrangers, des laboratoires publics ou privés.

AN IMPLICIT-EXPLICIT FINITE VOLUME SCHEME FOR THE FULLY NONLINEAR SERRE SYSTEM OF EQUATIONS

DENYS DUTYKH*, DIDIER CLAMOND, PAUL MILEWSKI, AND DIMITRIOS MITSOTAKIS

Abstract. After we derive the Serre system of equations of water wave theory from a generalized variational principle, we present some of its structural properties. We also propose a robust and accurate numerical scheme to solve these equations based on the finite volume method. The numerical discretization is validated by comparisons with analytical, experimental data or other numerical solutions obtained by a highly accurate pseudo-spectral method.

Contents

1. Introduction 1
2. Mathematical model 2
2.1. Derivation of the Serre equations 4
2.2. Invariants of the Serre equations 6
3. Finite volume scheme and numerical results 7
3.1. High order reconstruction 9
3.2. Treatment of the dispersive terms 10
4. Pseudo-spectral Fourier-type method for Serre equations 11
5. Numerical results 13
5.1. Convergence test and invariants preservation 13
5.2. Solitary wave interaction 14
5.3. Experimental validation 16
6. Conclusions 18
Acknowledgements 20
References 21

1. Introduction

The full water wave problem consisting of the Euler equations with free surface still is a very difficult problem to study theoretically and even numerically. Consequently, the water wave theory has always been developed through the derivation, analysis and comprehension of various approximate models (see the historical review of Craik [15] for

Key words and phrases. Serre equations; finite volumes; UNO scheme; IMEX scheme; spectral methods.
* Corresponding author.

more information). For this reason a plethora of approximate models have been derived under various physical assumptions. In this family, the Serre equations have a particular place and they are the subject of the present study. The Serre equations can be derived from the Euler equations, contrary to Boussinesq systems or the shallow water system, without the small amplitude or the hydrostatic assumptions respectively.

The Serre equations are named after François Serre, an engineer at École Nationale des Ponts et Chaussées, who derived this model for the first time in 1953 in his prominent paper entitled *"Contribution à l'étude des écoulements permanents et variables dans les canaux"* (see [44]). Later, these equations have been independently rediscovered by Su and Gardner [48] and by Green, Laws and Naghdi [25]. The extension of Serre equations for general uneven bathymetries was derived by Seabra-Santos *et al.* [43]. For some generalizations and new results we refer to recent studies by Barthélémy [7] and by Dias & Milewski [16].

A variety of numerical methods have been applied to discretize dispersive wave models and, more specifically, the Serre equations. A pseudo-spectral method was applied in [16], an implicit finite difference scheme in [38, 7] and a compact higher-order scheme in [10, 11]. Some Galerkin and Finite Element type methods have been successfully applied to Boussinesq-type equations [17, 39, 4, 3].

Recently, efficient high-order explicit or implicit-explicit finite volume schemes for dispersive wave equations have been developed [20, 19]. The robustness of the proposed numerical schemes allowed also the run-up of long waves on a beach with high accuracy [20]. The present study is a further extension of the finite volume method to the practically important case of the Serre equations.

The present paper is organized as follows. In Section 2 we provide a derivation of the Serre equations from a relaxed Lagrangian principle and discuss some structural properties of the governing equations. The rationale on the employed finite volume scheme are given in Section 3. A very accurate pseudo-spectral method for the numerical solution of the Serre equations is presented in Section 4. In Section 5, we present convergence tests and numerical experiments validating the model and the numerical schemes. Finally, the last Section 6 contains main conclusions of this study.

2. Mathematical model

Consider an ideal incompressible fluid of constant density ρ. The vertical projection of the fluid domain Ω is a subset of $\mathbb{R}^2$. The horizontal independent variables are denoted by $\boldsymbol{x} = (x_1, x_2)$ and the upward vertical one by y. The origin of the Cartesian coordinate system is chosen such that the surface $y = 0$ corresponds to the still water level. The fluid is bounded below by an impermeable bottom at $y = -d$ and above by an impermeable free surface at $y = \eta(\boldsymbol{x}, t)$. We assume that the total depth $h(\boldsymbol{x}, t) \equiv d + \eta(\boldsymbol{x}, t)$ remains positive $h(\boldsymbol{x}, t) \geqslant h_0 > 0$ at all times t. The sketch of the physical domain is shown in Figure 1.

Remark 1. *We make the classical assumption that the free surface is a graph $z = \eta(\boldsymbol{x}, t)$ of a single-valued function. This means in practice that we exclude some interesting phenomena, (e.g., wave breaking) which are out of the scope of this modeling paradigm.*

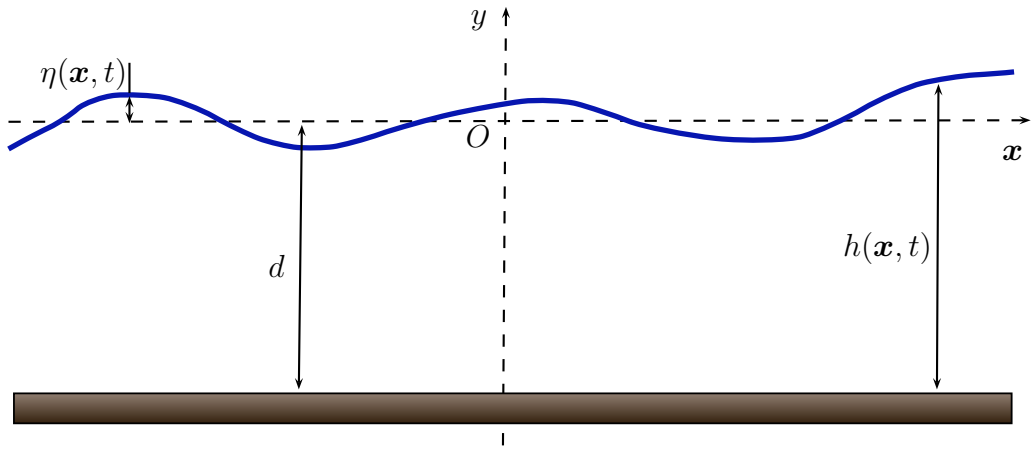

FIGURE 1. Sketch of the physical domain.

Assuming that the flow is incompressible and irrotational, the governing equations of the classical water wave problem are the following [30, 47, 35, 54]

$$\boldsymbol{\nabla}^2\phi \;+\; \partial_y^2\,\phi \;=\; 0 \qquad -\,d(\boldsymbol{x},t) \;\leqslant y \leqslant \eta(\boldsymbol{x},t), \tag{2.1}$$

$$\partial_t\eta \;+\; (\boldsymbol{\nabla}\phi)\cdot(\boldsymbol{\nabla}\eta) \;-\; \partial_y\,\phi \;=\; 0 \qquad y=\eta(\boldsymbol{x},t), \tag{2.2}$$

$$\partial_t\phi \;+\; \tfrac{1}{2}\,(\boldsymbol{\nabla}\phi)^2 \;+\; \tfrac{1}{2}\,(\partial_y\phi)^2 \;+\; g\,\eta \;=\; 0 \qquad y=\eta(\boldsymbol{x},t), \tag{2.3}$$

$$d_t \;+\; (\boldsymbol{\nabla}d)\cdot(\boldsymbol{\nabla}\phi) \;+\; \partial_y\,\phi \;=\; 0 \qquad y=-d(\boldsymbol{x},t), \tag{2.4}$$

with ϕ being the velocity potential (by definition, the irrotational velocity field $(\boldsymbol{u},v) = (\boldsymbol{\nabla}\phi,\partial_y\phi)$, g the acceleration due to gravity force and $\boldsymbol{\nabla} = (\partial_{x_1},\partial_{x_2})$ denotes the gradient operator in horizontal Cartesian coordinates.

The incompressibility condition leads to the Laplace equation for ϕ. The main difficulty of the water wave problem lies on the nonlinear free boundary conditions and that the free surface shape is unknown. Equations (2.2) and (2.4) express the free-surface kinematic condition and bottom impermeability respectively, while the dynamic condition (2.3) expresses the free surface isobarity.

The water wave problem possesses several variational structures [40, 53, 33, 56]. In the present study, we will focus mainly on the Lagrangian variational formalism but not exclusively. Surface gravity wave equations (2.1)–(2.4) can be derived by minimizing the following functional proposed by Luke [33]:

$$\mathcal{L} \;=\; \int_{t_1}^{t_2}\int_{\Omega}\mathscr{L}\,\rho\;\mathrm{d}^2\boldsymbol{x}\,\mathrm{d}t, \quad \mathscr{L} \;=\; -\int_{-d}^{\eta}\big[\,g\,y \;+\; \partial_t\,\phi \;+\; \tfrac{1}{2}\,(\boldsymbol{\nabla}\,\phi)^2 \;+\; \tfrac{1}{2}\,(\partial_y\,\phi)^2\,\big]\;\mathrm{d}y. \tag{2.5}$$

In a recent study, Clamond and Dutykh [12] proposed to use Luke's Lagrangian (2.5) in the following relaxed form

$$\begin{aligned}\mathscr{L} &= (\eta_t + \tilde{\boldsymbol{\mu}} \cdot \nabla\eta - \tilde{\nu})\,\tilde{\phi} \;+\; (d_t + \check{\boldsymbol{\mu}} \cdot \nabla d + \check{\nu})\,\check{\phi} \;-\; \tfrac{1}{2}\,g\,\eta^2 \\ &\quad + \int_{-d}^{\eta} \big[\,\boldsymbol{\mu} \cdot \boldsymbol{u} - \tfrac{1}{2}\boldsymbol{u}^2 \;+\; \nu v - \tfrac{1}{2}v^2 \;+\; (\nabla \cdot \boldsymbol{\mu} + \nu_y)\,\phi\,\big]\,\mathrm{d}y, \end{aligned} \tag{2.6}$$

where $\{\boldsymbol{u}, v, \boldsymbol{\mu}, \nu\}$ are the horizontal, vertical velocities and associated Lagrange multipliers, respectively. The additional variables $\{\boldsymbol{\mu}, \nu\}$ (Lagrange multipliers) are called pseudo-velocities. The over 'tildes' and 'wedges' denote, respectively, a quantity computed at the free surface $y = \eta(\boldsymbol{x}, t)$ and at the bottom $y = -d(\boldsymbol{x}, t)$. We shall also denote below with 'bars' the quantities averaged over the water depth.

While the original Lagrangian (2.5) incorporates only two variables (η and ϕ), the relaxed Lagrangian density (2.6) involves six variables $\{\eta, \phi, \boldsymbol{u}, v, \boldsymbol{\mu}, \nu\}$. These additional degrees of freedom provide us with more flexibility in constructing various approximations. For more details, explanations and examples we refer to [12].

2.1. **Derivation of the Serre equations.** Now we are going to illustrate the practical use of the variational principle (2.6) on an example borrowed from [12]. First of all, we choose a simple shallow water ansatz, which is a zeroth-order polynomial in y for ϕ and for $\boldsymbol{u}$, and a first-order one for v, i.e., we approximate flows that are nearly uniform along the vertical direction

$$\phi \;\approx\; \bar{\phi}(\boldsymbol{x}, t), \qquad \boldsymbol{u} \;\approx\; \bar{\boldsymbol{u}}(\boldsymbol{x}, t), \qquad v \;\approx\; (y + d)\,(\eta + d)^{-1}\,\tilde{v}(\boldsymbol{x}, t). \tag{2.7}$$

We have also to introduce suitable ansatz for the Lagrange multiplier $\boldsymbol{\mu}$ and ν

$$\boldsymbol{\mu} \;\approx\; \bar{\boldsymbol{\mu}}(\boldsymbol{x}, t), \qquad \nu \;\approx\; (y + d)\,(\eta + d)^{-1}\,\tilde{\nu}(\boldsymbol{x}, t).$$

In the remainder of this paper, we will assume for simplicity the bottom to be flat $d(\boldsymbol{x}, t) = d = \mathrm{Cst}$. With this ansatz the Lagrangian density (2.6) becomes

$$\begin{aligned}\mathscr{L} \;&=\; (\eta_t + \bar{\boldsymbol{\mu}} \cdot \boldsymbol{\nabla}\eta)\,\bar{\phi} \;-\; \tfrac{1}{2}\,g\,\eta^2 \\ &\quad + (\eta + d)\,\big[\,\bar{\boldsymbol{\mu}} \cdot \bar{\boldsymbol{u}} \;-\; \tfrac{1}{2}\,\bar{\boldsymbol{u}}^2 \;+\; \tfrac{1}{3}\,\tilde{\nu}\,\tilde{v} \;-\; \tfrac{1}{6}\,\tilde{v}^2 \;+\; \bar{\phi}\,\boldsymbol{\nabla} \cdot \bar{\boldsymbol{\mu}}\,\big]\,. \end{aligned} \tag{2.8}$$

Finally, we impose a constraint of the free surface impermeability, i.e.

$$\tilde{\nu} \;=\; \eta_t \;+\; \bar{\boldsymbol{\mu}} \cdot \boldsymbol{\nabla}\eta.$$

After substituting the last relation into the Lagrangian density (2.8), the minimization procedure leads to the following equations:

$$h_t \;+\; \boldsymbol{\nabla} \cdot [\,h\,\bar{\boldsymbol{u}}\,] \;=\; 0, \tag{2.9}$$

$$\begin{aligned}\bar{\boldsymbol{u}}_t \;+\; \bar{\boldsymbol{u}} \cdot \boldsymbol{\nabla}\bar{\boldsymbol{u}} \;+\; g\,\boldsymbol{\nabla}h \;+\; \tfrac{1}{3}\,h^{-1}\,\boldsymbol{\nabla}[\,h^2\,\tilde{\gamma}\,] \;&=\; (\bar{\boldsymbol{u}} \cdot \boldsymbol{\nabla}h)\,\boldsymbol{\nabla}(h\boldsymbol{\nabla} \cdot \bar{\boldsymbol{u}}) \\ &\quad -\; [\,\bar{\boldsymbol{u}} \cdot \boldsymbol{\nabla}(h\boldsymbol{\nabla} \cdot \bar{\boldsymbol{u}})\,]\,\boldsymbol{\nabla}h, \end{aligned} \tag{2.10}$$

where we eliminated $\bar{\phi}$, $\bar{\boldsymbol{\mu}}$ and $\tilde{v}$ and where

$$\tilde{\gamma} \;\equiv\; \tilde{v}_t \;+\; \bar{\boldsymbol{u}} \cdot \boldsymbol{\nabla}\tilde{v} \;=\; h\,\left\{\,(\boldsymbol{\nabla} \cdot \bar{\boldsymbol{u}})^2 \;-\; \boldsymbol{\nabla} \cdot \bar{\boldsymbol{u}}_t \;-\; \bar{\boldsymbol{u}} \cdot \boldsymbol{\nabla}\,[\,\boldsymbol{\nabla} \cdot \bar{\boldsymbol{u}}\,]\,\right\}, \tag{2.11}$$

is the fluid vertical acceleration at the free surface. The vertical velocity at the free surface $\tilde{v}$ can be expressed in terms of other variables as well, i.e.,

$$\tilde{v} \;=\; \frac{\eta_t \,+\, (\boldsymbol{\nabla}\bar{\phi})\cdot(\boldsymbol{\nabla}\eta)}{1 \,+\, \frac{1}{3}|\boldsymbol{\nabla}\eta|^2}.$$

In two dimensions (one horizontal dimension), the two terms on the right hand side of (2.10) vanish and the system (2.9), (2.10) reduces to the classical Serre equations [44].

Remark 2. *In the publication by Clamond and Dutykh* [12] *it is explained why equations* (2.9), (2.10) *cannot be obtained from the classical Luke's Lagrangian. Thus, a relaxed form of the Lagrangian density* (2.6) *is necessary for the variational derivation of the Serre equations* (2.9), (2.10) *(see also* [28] *&* [36]*).*

2.1.1. *Generalized Serre equations.* A further generalization of the Serre equations can be obtained if we modify slightly the shallow water ansatz (2.7) following again the ideas from [12]:

$$\phi \;\approx\; \bar{\phi}(x,t), \qquad u \;\approx\; \bar{u}(x,t), \qquad v \;\approx\; \left[\frac{y+d}{\eta+d}\right]^{\lambda} \tilde{v}(x,t).$$

In the following we consider for simplicity the two-dimensional case and pose $\mu = u$ and $\nu = v$ together with the constraint $\tilde{v} = \eta_t + \tilde{u}\eta_x$ (free surface impermeability). Thus, the Lagrangian desnity (2.6) becomes

$$\mathscr{L} \;=\; (\,h_t \,+\, [\,h\,\bar{u}\,]_x)\,\tilde{\phi} \,-\, \tfrac{1}{2}\,g\,\eta^2 \,+\, \tfrac{1}{2}\,h\,\bar{u}^2 \,+\, \tfrac{1}{2}\,\beta\,h\,(\,\eta_t \,+\, \bar{u}\,\eta_x\,)^2\,. \tag{2.12}$$

where $\beta = (2\lambda+1)^{-1}$. After some algebra, the Euler–Lagrange equations lead to the following equations

$$h_t \,+\, [\,h\,\bar{u}\,]_x \;=\; 0, \tag{2.13}$$

$$\bar{u}_t \,+\, \bar{u}\,\bar{u}_x \,+\, g\,h_x \,+\, \beta\,h^{-1}\,[\,h^2\,\tilde{\gamma}\,]_x \;=\; 0, \tag{2.14}$$

where $\tilde{\gamma}$ is defined as above (2.11). If $\beta = \frac{1}{3}$ (or equivalently $\lambda = 1$) the classical Serre equations (2.9), (2.10) are recovered.

Using equations (2.13) and (2.14) one can show that the following relations hold

$$[\,h\,\bar{u}\,]_t \,+\, \left[\,h\,\bar{u}^2 \,+\, \tfrac{1}{2}\,g\,h^2 \,+\, \beta\,h^2\,\tilde{\gamma}\,\right]_x \;=\; 0,$$

$$[\,\bar{u} \,-\, \beta\,h^{-1}(h^3\bar{u}_x)_x\,]_t \,+\, \left[\,\tfrac{1}{2}\,\bar{u}^2 \,+\, g\,h \,-\, \tfrac{1}{2}\,h^2\,\bar{u}_x^2 \,-\, \beta\,\bar{u}h^{-1}\,(h^3\bar{u}_x)_x\,\right]_x \;=\; 0,$$

$$[\,h\,\bar{u} \,-\, \beta\,(h^3\bar{u}_x)_x\,]_t \,+\, \left[\,h\,\bar{u}^2 \,+\, \tfrac{1}{2}\,g\,h^2 \,-\, 2\,\beta\,h^3\,\bar{u}_x^2 \,-\, \beta\,h^3\,\bar{u}\,\bar{u}_{xx} \,-\, h^2\,h_x\,\bar{u}\,\bar{u}_x\,\right]_x \;=\; 0,$$

$$\left[\,\tfrac{1}{2}\,h\,\bar{u}^2 \,+\, \tfrac{1}{2}\,\beta\,h^3\,\bar{u}_x^2 \,+\, \tfrac{1}{2}\,g\,h^2\,\right]_t \,+\, \left[\,\left(\,\tfrac{1}{2}\,\bar{u}^2 \,+\, \tfrac{1}{2}\,\beta\,h^2\,\bar{u}_x^2 \,+\, g\,h \,+\, \beta\,h\,\tilde{\gamma}\,\right)h\,\bar{u}\,\right]_x \;=\; 0.$$

Physically, these relations represent conservations of the momentum, potential vorticity [36], potential vorticity flux and energy, respectivelyy. Moreover, the Serre equations are invariant under the Galilean transformation. This property is naturally inherited from the full water wave problem since our ansatz does not destroy this symmetry [8] and the derivation is made according variational principles.

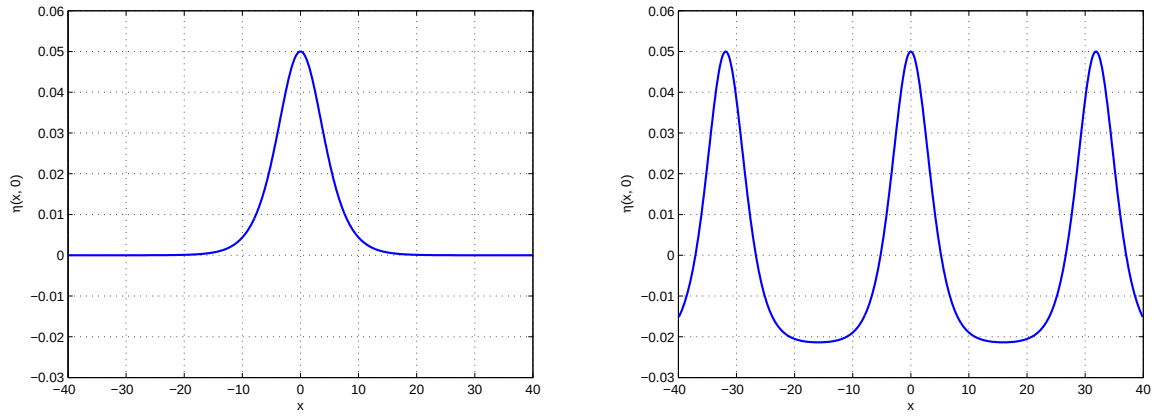

(a) Solitary wave (b) Cnoidal wave

FIGURE 2. Two exact solutions to Serre equations. For the cnoidal wave parameters m and a are equal to 0.99 and 0.05 respectively.

Equations (2.13)–(2.14) admit a $(2\pi/k)$-periodic cnoidal traveling wave solution

$$\bar{u} \;=\; \frac{c\,\eta}{d+\eta}, \tag{2.15}$$

$$\eta \;=\; a\,\frac{\mathrm{dn}^2\big(\frac{1}{2}\varkappa(x-ct)|m\big) - E/K}{1-E/K} \;=\; a \;-\; H\;\mathrm{sn}^2\big(\tfrac{1}{2}\varkappa(x-ct)|m\big)\,, \tag{2.16}$$

where dn and sn are the Jacobian elliptic functions with parameter m $(0 \leqslant m \leqslant 1)$, and where $K = \mathrm{K}(m)$ and $E = \mathrm{E}(m)$ are the complete ellipic integrals of the first and second kind, respectively [1]. The wave parameters are given by the relations

$$k \;=\; \frac{\pi\,\varkappa}{2\,K}, \qquad H \;=\; \frac{m\,a\,K}{K-E}, \qquad (\varkappa d)^2 \;=\; \frac{g\,H}{m\,\beta\,c^2}, \tag{2.17}$$

$$m \;=\; \frac{g\,H\,(d+a)\,(d+a-H)}{g\,(d+a)^2\,(d+a-H) \;-\; d^2\,c^2}. \tag{2.18}$$

However, in the present study, we are interested in the classical solitary wave solution which is recovered in the limiting case $m \to 1$

$$\eta = a\;\mathrm{sech}^2\tfrac{1}{2}k(x-ct), \quad \bar{u} = \frac{c\,\eta}{d+\eta}, \quad c^2 = g(d+a), \quad (kd)^2 = \frac{a}{\beta(d+a)}. \tag{2.19}$$

For illustrative purposes, some free surface elevations are depicted on Figure 2.

2.2. **Invariants of the Serre equations.** Henceforth we consider only the two-dimensional case. As pointed out by Yi Li (2002) [31], the classical Serre equations possess a non-canonical Hamiltonian structure which can be easily generalized for the model (2.13),

(2.14)

$$\begin{pmatrix} h_t \\ \tilde{q}_t \end{pmatrix} \;=\; \mathbb{J} \cdot \begin{pmatrix} \delta\,\mathcal{H}\,/\,\delta\tilde{q} \\ \delta\,\mathcal{H}\,/\,\delta h \end{pmatrix},$$

where the Hamiltonian functional $\mathcal{H}$ and the symplectic operator $\mathbb{J}$ are defined as

$$\mathcal{H} \;=\; \tfrac{1}{2}\int_{\mathbb{R}} \Big[\, h\,\bar{u}^2 \,+\, \beta\, h^3\,\bar{u}_x^2 \,+\, g\,\eta^2 \,\Big]\,\mathrm{d}x, \qquad \mathbb{J} \;=\; -\begin{pmatrix} h_x & 0 \\ \tilde{q}_x + \tilde{q}\partial_x & h\partial_x \end{pmatrix}.$$

The variable $\tilde{q}$ is sometimes referred to as the *potential vorticity flux* and is defined by

$$\tilde{q} \;\equiv\; h\,\bar{u} \;-\; \beta\,[\,h^3\,\bar{u}_x\,]_x.$$

According to [31], one-parameter symmetry groups of Serre equations include the space translation $(x+\varepsilon, t, h, u)$, the time translation $(x, t+\varepsilon, h, u)$, the Galilean boost $(x + \varepsilon t, t, h, u+\varepsilon)$ and the scaling $\mathrm{e}^{\varepsilon}(\mathrm{e}^{\varepsilon}x, t, \mathrm{e}^{\varepsilon}h, u)$. Using the first three symmetry groups and the symplectic operator $\mathbb{J}$, one may recover the following invariants:

$$Q \;=\; \int_{\mathbb{R}} \frac{\eta\,\tilde{q}}{d\,+\,\eta}\,\mathrm{d}x, \qquad \mathcal{H}, \qquad \int_{\mathbb{R}} \big[\, t\,\tilde{q} \,-\, x\,\eta\,\big]\,\mathrm{d}x. \tag{2.20}$$

Obviously, the equation (2.13) leads to an invariant closely related to the mass conservation property $\int_{\mathbb{R}} \eta\,\mathrm{d}x$. The scaling does not yield any conserved quantity with respect to the symplectic operator $\mathbb{J}$. Below, we are going to use extensively the generalized energy $\mathcal{H}$ and the generalized momentum Q conservation to assess the accuracy of the numerical schemes additionally to the exact analytical solution (2.19).

3. Finite volume scheme and numerical results

In the present study, we propose a finite volume discretization procedure [5, 6] for the following Serre equations

$$h_t \;+\; [\,h\,u\,]_x \;=0, \tag{3.1}$$

$$u_t \;+\; \big[\,\tfrac{1}{2}\,u^2 \,+\, g\,h\,\big]_x \;=\beta\,h^{-1}\,\big[\,h^3\,(u_{xt} \,+\, u\,u_{xx} \,-\, u_x^2)\,\big]_x, \tag{3.2}$$

where the overlines have been omitted for brevity. (In this section, overlines denote quantities averaged over a cell, as explained below.)

We begin our presentation by a discretization of the hyperbolic part of the equations (which are simply the classical Saint-Venant equations) and then discuss the treatment of dispersive terms. The Serre equations can be formally put under the quasilinear form

$$\boldsymbol{V}_t \;+\; [\,\boldsymbol{F}(\boldsymbol{V})\,]_x \;=\; \boldsymbol{S}(\boldsymbol{V}), \tag{3.3}$$

where $\boldsymbol{V}$, $\boldsymbol{F}(\boldsymbol{V})$ are the conservative variables and the advective flux function, respectively

$$\boldsymbol{V} \;\equiv\; \begin{pmatrix} h \\ u \end{pmatrix}, \quad \boldsymbol{F}(\boldsymbol{V}) \;\equiv\; \begin{pmatrix} h\,u \\ \frac{1}{2}\,u^2 \,+\, g\,h \end{pmatrix}.$$

The source term $\boldsymbol{S}(\boldsymbol{V})$ denotes the right-hand side of (3.1), (3.2) and thus, depends also on space and time derivatives of $\boldsymbol{V}$.

The Jacobian of the advective flux $\boldsymbol{F}(\boldsymbol{V})$ can be easily computed

$$\mathbb{A}(\boldsymbol{V}) \;=\; \frac{\partial\,\boldsymbol{F}(\boldsymbol{V})}{\partial \boldsymbol{V}} \;=\; \begin{pmatrix} u & h \\ g & u \end{pmatrix}.$$

The Jacobian $\mathbb{A}(\boldsymbol{V})$ has two distinctive eigenvalues

$$\lambda^{\pm} \;=\; u \;\pm\; c_s, \qquad c_s \;\equiv\; \sqrt{gh}.$$

The corresponding right and left eigenvectors are provided here

$$\mathbb{R} \;=\; \begin{pmatrix} h & -h \\ c_s & c_s \end{pmatrix}, \qquad \mathbb{L} \;=\; \mathbb{R}^{-1} \;=\; \frac{1}{2}\begin{pmatrix} h^{-1} & c_s^{-1} \\ -h^{-1} & c_s^{-1} \end{pmatrix}.$$

We consider a partition of $\mathbb{R}$ into cells (or finite volumes) $\mathcal{C}_i = [x_{i-\frac{1}{2}}, x_{i+\frac{1}{2}}]$ with cell centers $x_i = \frac{1}{2}(x_{i-\frac{1}{2}} + x_{i+\frac{1}{2}})$ $(i \in \mathbb{Z})$. Let Δx_i denotes the length of the cell $\mathcal{C}_i$. In the sequel we will consider only uniform partitions with $\Delta x_i = \Delta x$, $\forall i \in \mathbb{Z}$. We would like to approximate the solution $\boldsymbol{V}(x,t)$ by discrete values. In order to do so, we introduce the cell average of $\boldsymbol{V}$ on the cell $\mathcal{C}_i$ (denoted with an overline), i.e.,

$$\bar{\boldsymbol{V}}_i(t) \;\equiv\; \big(\,\bar{h}(t)\,,\,\bar{u}(t)\,\big) \;=\; \frac{1}{\Delta x}\int_{\mathcal{C}_i} \boldsymbol{V}(x,t)\,\mathrm{d}x.$$

A simple integration of (3.3) over the cell $\mathcal{C}_i$ leads the following exact relation:

$$\frac{\mathrm{d}\,\bar{\boldsymbol{V}}}{\mathrm{d}t} \;+\; \frac{1}{\Delta x}\Big[\,\boldsymbol{F}(\boldsymbol{V}(x_{i+\frac{1}{2}},t)) \;-\; \boldsymbol{F}(\boldsymbol{V}(x_{i-\frac{1}{2}},t))\,\Big] \;=\; \frac{1}{\Delta x}\int_{\mathcal{C}_i} \boldsymbol{S}(\boldsymbol{V})\,\mathrm{d}x \;\equiv\; \bar{\boldsymbol{S}}_i.$$

Since the discrete solution is discontinuous at cell interfaces $x_{i+\frac{1}{2}}$ $(i \in \mathbb{Z})$, we replace the flux at the cell faces by the so-called numerical flux function

$$\boldsymbol{F}(\boldsymbol{V}(x_{i\pm\frac{1}{2}},t)) \;\approx\; \boldsymbol{\mathcal{F}}_{i\pm\frac{1}{2}}(\bar{\boldsymbol{V}}^{L}_{i\pm\frac{1}{2}}, \bar{\boldsymbol{V}}^{R}_{i\pm\frac{1}{2}}),$$

where $\bar{\boldsymbol{V}}^{L,R}_{i\pm\frac{1}{2}}$ denotes the reconstructed of the conservative variables $\bar{\boldsymbol{V}}$ from left and right sides of each cell interface (the reconstruction procedure employed in the present study will be described below). Consequently, the semi-discrete scheme takes the form

$$\frac{\mathrm{d}\,\bar{\boldsymbol{V}}_i}{\mathrm{d}t} \;+\; \frac{1}{\Delta x}\big[\,\boldsymbol{\mathcal{F}}_{i+\frac{1}{2}} \;-\; \boldsymbol{\mathcal{F}}_{i-\frac{1}{2}}\,\big] \;=\; \bar{\boldsymbol{S}}_i. \tag{3.4}$$

In order to discretize the advective flux $\boldsymbol{F}(\boldsymbol{V})$, we use the FVCF scheme [23, 24]:

$$\boldsymbol{\mathcal{F}}(\boldsymbol{V},\boldsymbol{W}) \;=\; \frac{\boldsymbol{F}(\boldsymbol{V}) \;+\; \boldsymbol{F}(\boldsymbol{W})}{2} \;-\; \mathbb{U}(\boldsymbol{V},\boldsymbol{W})\cdot\frac{\boldsymbol{F}(\boldsymbol{W}) \;-\; \boldsymbol{F}(\boldsymbol{V})}{2}.$$

The first part of the numerical flux is centered, the second part is the upwinding introduced through the Jacobian sign-matrix $\mathbb{U}(\boldsymbol{V},\boldsymbol{W})$ defined as

$$\mathbb{U}(\boldsymbol{V},\boldsymbol{W}) \;=\; \mathrm{sign}\big[\mathbb{A}(\tfrac{1}{2}(\boldsymbol{V}+\boldsymbol{W}))\big], \qquad \mathrm{sign}(\mathbb{A}) \;=\; \mathbb{R}\cdot\mathrm{diag}(s^{+},s^{-})\cdot\mathbb{L},$$

where $s^{\pm} \equiv \mathrm{sign}(\lambda^{\pm})$. After some simple algebraic computations, one can find

$$\mathbb{U} \;=\; \frac{1}{2}\begin{pmatrix} s^{+}+s^{-} & (h/c_s)\,(s^{+}-s^{-}) \\ (c_s/h)\,(s^{+}-s^{-}) & s^{+}+s^{-} \end{pmatrix},$$

the sign-matrix $\mathbb{U}$ being evaluated at the average state of left and right values.

3.1. **High order reconstruction.** In order to obtain a higher-order scheme in space, we need to replace the piecewise constant data by a piecewise polynomial representation. This goal is achieved by various so-called reconstruction procedures such as MUSCL TVD [29, 50, 51], UNO [27], ENO [26], WENO [55] and many others. In our previous study on Boussinesq-type equations [20], the UNO2 scheme showed a good performance with small dissipation in realistic propagation and runup simulations. Consequently, we retain this scheme for the discretization of the advective flux in Serre equations.

Remark 3. *In TVD schemes, the numerical operator is required (by definition) not to increase the total variation of the numerical solution at each time step. It follows that the value of an isolated maximum may only decrease in time which is not a good property for the simulation of coherent structures such as solitary waves. The nonoscillatory UNO2 scheme, employed in our study, is only required to diminish the* number *of local extrema in the numerical solution. Unlike TVD schemes, UNO schemes are not constrained to damp the values of each local extremum at every time step.*

The main idea of the UNO2 scheme is to construct a non-oscillatory piecewise-parabolic interpolant $\boldsymbol{Q}(x)$ to a piecewise smooth function $\boldsymbol{V}(x)$ (see [27] for more details). On each segment containing the face $x_{i+\frac{1}{2}} \in [x_i, x_{i+1}]$, the function $\boldsymbol{Q}(x) = \boldsymbol{q}_{i+\frac{1}{2}}(x)$ is locally a quadratic polynomial and wherever $v(x)$ is smooth we have

$$\boldsymbol{Q}(x) \;-\; \boldsymbol{V}(x) \;=\; \boldsymbol{0} \;+\; \mathcal{O}(\Delta x^3), \qquad \frac{\mathrm{d}\,\boldsymbol{Q}}{\mathrm{d}x}(x \pm 0) \;-\; \frac{\mathrm{d}\,\boldsymbol{V}}{\mathrm{d}x} \;=\; \boldsymbol{0} \;+\; \mathcal{O}(\Delta x^2).$$

Also, $\boldsymbol{Q}(x)$ should be non-oscillatory in the sense that the number of its local extrema does not exceed that of $\boldsymbol{V}(x)$. Since $\boldsymbol{q}_{i+\frac{1}{2}}(x_i) = \bar{\boldsymbol{V}}_i$ and $\boldsymbol{q}_{i+\frac{1}{2}}(x_{i+1}) = \bar{\boldsymbol{V}}_{i+1}$, it can be written in the form

$$\boldsymbol{q}_{i+\frac{1}{2}}(x) \;=\; \bar{\boldsymbol{V}}_i \;+\; \mathfrak{d}_{i+\frac{1}{2}}\{\boldsymbol{V}\} \times \frac{x - x_i}{\Delta x} \;+\; \tfrac{1}{2}\,\mathfrak{D}_{i+\frac{1}{2}}\{\boldsymbol{V}\} \times \frac{(x - x_i)(x - x_{i+1})}{\Delta x^2},$$

where $\mathfrak{d}_{i+\frac{1}{2}}\{\boldsymbol{V}\} \equiv \bar{\boldsymbol{V}}_{i+1} - \bar{\boldsymbol{V}}_i$ and $\mathfrak{D}_{i+\frac{1}{2}}\boldsymbol{V}$ is closely related to the second derivative of the interpolant since $\mathfrak{D}_{i+\frac{1}{2}}\{\boldsymbol{V}\} = \Delta x^2\, \boldsymbol{q}''_{i+\frac{1}{2}}(x)$. The polynomial $\boldsymbol{q}_{i+\frac{1}{2}}(x)$ is chosen to be the least oscillatory between two candidates interpolating $\boldsymbol{V}(x)$ at (x_{i-1}, x_i, x_{i+1}) and (x_i, x_{i+1}, x_{i+2}). This requirement leads to the following choice of $\mathfrak{D}_{i+\frac{1}{2}}\{\boldsymbol{V}\} \equiv \mathrm{minmod}\big(\mathfrak{D}_i\{\boldsymbol{V}\}, \mathfrak{D}_{i+1}\{\boldsymbol{V}\}\big)$ with

$$\mathfrak{D}_i\{\boldsymbol{V}\} \;=\; \bar{\boldsymbol{V}}_{i+1} \;-\; 2\,\bar{\boldsymbol{V}}_i \;+\; \bar{\boldsymbol{V}}_{i-1}, \qquad \mathfrak{D}_{i+1}\{\boldsymbol{V}\} \;=\; \bar{\boldsymbol{V}}_{i+2} \;-\; 2\,\bar{\boldsymbol{V}}_{i+1} \;+\; \bar{\boldsymbol{V}}_i,$$

and where $\mathrm{minmod}(x, y)$ is the usual minmod function defined as

$$\mathrm{minmod}(x, y) \;\equiv\; \tfrac{1}{2}\,[\,\mathrm{sign}(x) \;+\; \mathrm{sign}(y)\,] \times \min(|x|, |y|).$$

To achieve the second order $\mathcal{O}(\Delta x^2)$ accuracy, it is sufficient to consider piecewise linear reconstructions in each cell. Let $L(x)$ denote this approximately reconstructed function

which can be written in this form

$$L(x) \;=\; \bar{\boldsymbol{V}}_i \;+\; \boldsymbol{S}_i \cdot \frac{x - x_i}{\Delta x}, \qquad x \in [x_{i-\frac{1}{2}}, x_{i+\frac{1}{2}}].$$

In order to $L(x)$ be a non-oscillatory approximation, we use the parabolic interpolation $\boldsymbol{Q}(x)$ constructed below to estimate the slopes $\boldsymbol{S}_i$ within each cell

$$\boldsymbol{S}_i \;=\; \Delta x \times \mathrm{minmod}\Big(\frac{\mathrm{d}\,\boldsymbol{Q}}{\mathrm{d}x}(x_i - 0), \frac{\mathrm{d}\,\boldsymbol{Q}}{\mathrm{d}x}(x_i + 0)\Big).$$

In other words, the solution is reconstructed on the cells while the solution gradient is estimated on the dual mesh as it is often performed in more modern schemes [5, 6]. A brief summary of the UNO2 reconstruction can be also found in [20].

3.2. **Treatment of the dispersive terms.** In this section, we explain how we treat the dispersive terms of Serre equations (3.1), (3.2). We begin the exposition by discussing the space discretization and then, we propose a way to remove the intrinsic stiffness of the dispersion by partial implicitation.

For the sake of simplicity, we split the dispersive terms into three parts:

$$\mathbb{M}(\boldsymbol{V}) \;\equiv\; \beta\, h^{-1}\left[\, h^3\, u_{xt}\,\right]_x, \quad \mathbb{D}_1(\boldsymbol{V}) \;\equiv\; \beta\, h^{-1}\left[\, h^3\, u\, u_{xx}\,\right]_x, \quad \mathbb{D}_2(\boldsymbol{V}) \;\equiv\; \beta\, h^{-1}\left[\, h^3\, u_x^2\,\right]_x.$$

We propose the following approximations in space (which are all of the second order $\mathcal{O}(\Delta x^2)$ to be consistent with UNO2 advective flux discretization presented above)

$$\begin{aligned}
\mathbb{M}_i(\bar{\boldsymbol{V}}) \;&=\; \beta\, \bar{h}_i^{-1}\, \frac{\bar{h}_{i+1}^3\, (\bar{u}_{xt})_{i+1} \;-\; \bar{h}_{i-1}^3\, (\bar{u}_{xt})_{i-1}}{2\,\Delta x} \\
&=\; \frac{\beta\, \bar{h}_i^{-1}}{2\,\Delta x}\left[\, \bar{h}_{i+1}^3\, \frac{(\bar{u}_t)_{i+2} \;-\; (\bar{u}_t)_i}{2\,\Delta x} \;-\; \bar{h}_{i-1}^3\, \frac{(\bar{u}_t)_i \;-\; (\bar{u}_t)_{i-2}}{2\,\Delta x}\,\right] \\
&=\; \frac{\beta\, \bar{h}_i^{-1}}{4\,\Delta x^2}\left[\, \bar{h}_{i+1}^3\, (\bar{u}_t)_{i+2} \;-\; (\bar{h}_{i+1}^3 \;+\; \bar{h}_{i-1}^3)\, (\bar{u}_t)_i \;+\; \bar{h}_{i-1}^3\, (\bar{u}_t)_{i-2}\,\right].
\end{aligned}$$

The last relation can be rewritten in a short-hand form if we introduce the matrix $\mathbb{M}(\bar{\boldsymbol{V}})$ such that the i-th component of the product $\mathbb{M}(\bar{\boldsymbol{V}}) \cdot \bar{\boldsymbol{V}}_t$ gives exactly the expression $\mathbb{M}_i(\bar{\boldsymbol{V}})$.

In a similar way, we discretize the other dispersive terms without giving here the intermediate steps

$$\begin{aligned}
\mathbb{D}_{1i}(\bar{\boldsymbol{V}}) \;&=\; \frac{\beta\, \bar{h}_i^{-1}}{2\,\Delta x^2}\left[\, \bar{h}_{i+1}^3\, \bar{u}_{i+1}\, (\bar{u}_{i+2} - 2\bar{u}_{i+1} + \bar{u}_i) \;-\; \bar{h}_{i-1}^3\, \bar{u}_{i-1}\, (\bar{u}_i - 2\bar{u}_{i-1} + \bar{u}_{i-2})\,\right], \\
\mathbb{D}_{2i}(\bar{\boldsymbol{V}}) \;&=\; \frac{\beta \bar{h}_i^{-1}}{8\Delta x^3}\left[\, \bar{h}_{i+1}^3\, (\bar{u}_{i+2} - \bar{u}_i)^2 \;-\; \bar{h}_{i-1}^3\, (\bar{u}_i - \bar{u}_{i-2})^2\,\right].
\end{aligned}$$

If we denote by $\mathbb{I}$ the identity matrix, we can rewrite the semi-discrete scheme (3.4) by expanding the right-hand side $\boldsymbol{S}_i$

$$\begin{aligned}
\frac{\mathrm{d}\,\bar{h}}{\mathrm{d}t} \;+\; \frac{1}{\Delta x}\left[\, \mathcal{F}_+^{(1)}(\bar{\boldsymbol{V}}) \;-\; \mathcal{F}_-^{(1)}(\bar{\boldsymbol{V}})\,\right] \;&=\; 0, \\
(\mathbb{I} - \mathbb{M}) \cdot \frac{\mathrm{d}\,\bar{u}}{\mathrm{d}t} \;+\; \frac{1}{\Delta x}\left[\, \mathcal{F}_+^{(2)}(\bar{\boldsymbol{V}}) \;-\; \mathcal{F}_-^{(2)}(\bar{\boldsymbol{V}})\,\right] \;&=\; \mathbb{D}(\bar{\boldsymbol{V}}) \cdot \bar{u},
\end{aligned}$$

where $\mathcal{F}_{\pm}^{(1,2)}(\bar{\boldsymbol{V}})$ are the two components of the advective numerical flux vector $\boldsymbol{\mathcal{F}}$ at the right $(+)$ and left $(-)$ faces correspondingly and $\mathbb{D}(\bar{\boldsymbol{V}}) \equiv \mathbb{D}_1(\bar{\boldsymbol{V}}) - \mathbb{D}_2(\bar{\boldsymbol{V}})$.

Finally, in order to describe the fully discrete scheme, we need to specify how we distribute the nonlinear terms in expressions $\mathbb{D}_{1,2}(\bar{v})$ on time layers t_n and t_{n+1}. We will perform it in an economical way so that on each time step we have only one linear system to solve

$$\begin{aligned}\big[\,\mathbb{D}_1(\bar{\boldsymbol{V}}^{(n)})\cdot\bar{u}^{(n+1)}\,\big]_i \;&=\; \frac{\beta}{2\,h_i^{(n)}\,\Delta x^2}\,\big[\,(h_{i+1}^{(n)})^3\,\bar{u}_{i+1}^{(n)}\,(\bar{u}_{i+2}^{(n+1)}-2\bar{u}_{i+1}^{(n+1)}+\bar{u}_i^{(n+1)})\\ &\quad-\;(h_{i-1}^{(n)})^3\,\bar{u}_{i-1}^{(n)}\,(\bar{u}_i^{(n+1)}-2\bar{u}_{i-1}^{(n+1)}+\bar{u}_{i-2}^{(n+1)})\,\big],\end{aligned}$$

$$\begin{aligned}\big[\,\mathbb{D}_2(\bar{\boldsymbol{V}}^{(n)})\cdot\bar{u}^{(n+1)}\,\big]_i \;&=\; \frac{\beta}{8\,h_i^{(n)}\,\Delta x^3}\,\big[\,(h_{i+1}^{(n)})^3\,(\bar{u}_{i+2}^{(n)}-\bar{u}_i^{(n)})(\bar{u}_{i+2}^{(n+1)}-\bar{u}_i^{(n+1)})\\ &\quad-\;(h_{i-1}^{(n)})^3\,(\bar{u}_i^{(n)}-\bar{u}_{i-2}^{(n)})(\bar{u}_i^{(n+1)}-\bar{u}_{i-2}^{(n+1)})\,\big].\end{aligned}$$

In our numerical scheme, the advective terms will be treated in the explicit way since the reconstruction procedure is relatively complex and, therefore, highly nonlinear. Consequently, the fully discrete scheme takes the following form:

$$\bar{h}^{(n+1)} \;=\; \bar{h}^{(n)} \;-\; \frac{\Delta t}{\Delta x}\,\big[\,\mathcal{F}_{+}^{(1)}(\bar{\boldsymbol{V}}^{(n)}) \;-\; \mathcal{F}_{-}^{(1)}(\bar{\boldsymbol{V}}^{(n)})\,\big], \tag{3.5}$$

$$(\,\mathbb{I}\,-\,\mathbb{M}\,-\,\Delta t\,\mathbb{D}\,)\cdot\bar{u}^{(n+1)} \;=\; (\,\mathbb{I}\,-\,\mathbb{M}\,)\cdot\bar{u}^{(n)} \;-\; \frac{\Delta t}{\Delta x}\,\big[\,\mathcal{F}_{+}^{(2)}(\bar{\boldsymbol{V}}^{(n)}) \;-\; \mathcal{F}_{-}^{(2)}(\bar{\boldsymbol{V}}^{(n)})\,\big], \tag{3.6}$$

where Δt is the chosen time step and the matrix $\mathbb{D} \equiv \mathbb{D}_1 - \mathbb{D}_2$ as above.

Remark 4. *It is possible to enhance the time discretization accuracy by applying the Richardson extrapolation technique* [21]*, for example. Let us briefly recall the main idea. It consists in approximating the solution $\bar{v}(t)$ with two time steps $\bar{v}_{\Delta t}$ and $\bar{v}_{\Delta t/2}$. Since the fully discrete scheme* (3.5)*,* (3.6) *is* locally *second order accurate, the Richardson extrapolation technique aims to cancel the leading error term by taking the following combination:*

$$\bar{v}(t) \;\approx\; \tfrac{4}{3}\,\bar{v}_{\Delta t/2} \;-\; \tfrac{1}{3}\,\bar{v}_{\Delta t}.$$

4. Pseudo-spectral Fourier-type method for Serre equations

In this Section we describe a pseudo-spectral solver to integrate numerically the Serre equations in periodic domains. In spectral methods it is more convenient to work in variables free surface elevation $\eta(x,t)$ and potential vorticity $q(x,t)$

$$\eta_t \;+\; \big[\,(d+\eta)\,\bar{u}\,\big]_x \;=\; 0, \tag{4.1}$$

$$q_t \;+\; \big[\,q\,u \;-\; \tfrac{1}{2}\,\bar{u}^2 \;+\; g\,\eta \;-\; \tfrac{1}{2}\,(d+\eta)^2\,\bar{u}_x^2\,\big]_x \;=\; 0, \tag{4.2}$$

$$q \;-\; \bar{u} \;+\; \tfrac{1}{3}(d+\eta)^2\bar{u}_{xx} \;+\; (d+\eta)\eta_x\bar{u}_x \;=\; 0. \tag{4.3}$$

The first two equations (4.1), (4.2) are of evolution type, while the third one (4.3) relates the potential vorticity q to the primitive variables: the free surface elevation η and the

velocity $\bar{u}$. In order to solve relation (4.3) with respect to the velocity $\bar{u}$, we extract the linear part as

$$\bar{u} \;-\; \tfrac{1}{3}\, d^2\, \bar{u}_{xx} \;-\; q \;=\; \underbrace{\tfrac{1}{3}\,(2d\eta + \eta^2)\,\bar{u}_{xx} \;+\; (d+\eta)\,\eta_x\,\bar{u}_x}_{N(\eta,\bar{u})}.$$

Then, we apply to the last relation the following fixed point type iteration in Fourier space

$$\hat{\bar{u}}_{j+1} \;=\; \frac{\hat{q}}{1+\frac{1}{3}(kd)^2} \;+\; \frac{\boldsymbol{\mathcal{F}}\big\{N(\eta,\bar{u}_j)\big\}}{1+\frac{1}{3}(kd)^2} \qquad j = 0, 1, 2, \cdots, \tag{4.4}$$

where $\hat{\psi} \equiv \boldsymbol{\mathcal{F}}\{\psi\}$ denotes the Fourier transform of a quantity ψ. The last iteration continues until the desired convergence. For example, for moderate amplitude solitary waves (≈ 0.2), the accuracy 10^{-16} is attained in approximatively 20 iterations if the velocity $\bar{u}_0$ is initialized from the previous time step. We note that the usual 4-half rule is applied to the nonlinear terms for anti-aliasing [49, 13, 22].

In order to improve the numerical stability of the time stepping method, we will integrate exactly the linear terms in evolution equations

$$\begin{aligned} \eta_t \;+\; d\,\bar{u}_x \;&=\; -\big[\,\eta\,\bar{u}\,\big]_x, \\ q_t \;+\; g\,\eta_x \;&=\; \Big[\,\tfrac{1}{2}\,\bar{u}^2 \;+\; \tfrac{1}{2}\,(d+\eta)^2\,\bar{u}_x^2 \;-\; q\,u\,\Big]_x. \end{aligned}$$

Taking the Fourier transform and using the relation (4.3) between $\bar{u}$ and q, we obtain the following system of ODEs:

$$\begin{aligned} \hat{\eta}_t \;+\; \frac{\mathrm{i}kd}{1+\frac{1}{3}(kd)^2}\,\hat{q} \;&=\; -\,\mathrm{i}k\,\boldsymbol{\mathcal{F}}\{\eta\bar{u}\} \;-\; \frac{\mathrm{i}kd\,\boldsymbol{\mathcal{F}}\big\{N(\eta,\bar{u}_j)\big\}}{1+\frac{1}{3}(kd)^2}, \\ \hat{q}_t \;+\; \mathrm{i}kg\,\hat{\eta} \;&=\; \mathrm{i}k\,\boldsymbol{\mathcal{F}}\big\{\,\tfrac{1}{2}\bar{u}^2 \;+\; \tfrac{1}{2}(d+\eta)^2\bar{u}_x^2 \;-\; qu\,\big\}. \end{aligned}$$

The next step consists in introducing the vector of dimensionless variables in Fourier space $\hat{\boldsymbol{V}} \equiv (\mathrm{i}k\hat{\eta}, \dfrac{\mathrm{i}\omega}{g}\hat{q})$, where $\omega^2 = \dfrac{gk^2d}{1+\frac{1}{3}(kd)^2}$ is the dispersion relation of the linearized Serre equations. With unscaled variables in vectorial form, the last system becomes

$$\hat{\boldsymbol{V}}_t \;+\; \mathbb{L}\cdot\hat{\boldsymbol{V}} \;=\; \boldsymbol{N}(\hat{\boldsymbol{V}}), \qquad \mathbb{L} \;\equiv\; \begin{pmatrix} 0 & \mathrm{i}\omega \\ \mathrm{i}\omega & 0 \end{pmatrix}.$$

On the right-hand side, we put all the nonlinear terms

$$\boldsymbol{N}(\hat{\boldsymbol{V}}) \;=\; \begin{pmatrix} k^2\,\boldsymbol{\mathcal{F}}\{\eta\bar{u}\} \;+\; dk^2\,\boldsymbol{\mathcal{F}}\big\{N(\eta,\bar{u}_j)\big\}/(1+\frac{1}{3}(kd)^2) \\ -(k\omega/g)\,\boldsymbol{\mathcal{F}}\big\{\frac{1}{2}\bar{u}^2 \;+\; \frac{1}{2}(d+\eta)^2\bar{u}_x^2 \;-\; qu\big\} \end{pmatrix}.$$

In order to integrate the linear terms, we make the last change of variables [37, 22]:

$$\hat{\boldsymbol{W}}_t \;=\; \mathrm{e}^{(t-t_0)\mathbb{L}}\cdot\boldsymbol{N}\Big\{\mathrm{e}^{-(t-t_0)\mathbb{L}}\cdot\hat{\boldsymbol{W}}\Big\}, \qquad \hat{\boldsymbol{W}}(t) \;\equiv\; \mathrm{e}^{-(t-t_0)\mathbb{L}}\cdot\hat{\boldsymbol{V}}(t), \qquad \hat{\boldsymbol{W}}(t_0) \;=\; \hat{\boldsymbol{V}}(t_0).$$

Finally, the last system of ODEs is discretized in time by Verner's embedded adaptive 9(8) Runge–Kutta scheme [52]. The time step is chosen adaptively using the so-called H211b

Undisturbed water depth: d	1
Gravity acceleration: g	1
Solitary wave amplitude: a	0.05
Final simulation time: T	2
Free parameter: β	1/3

TABLE 1. Values of various parameters used in convergence tests.

digital filter [45, 46] to meet some estimated error tolerance (generally of the same order of the fixed point iteration (4.4) precision).

5. Numerical results

In the present section we present some numerical results the new finite volume scheme. First, we validate the discretization and check the convergence of the scheme using an analytical solution. Then we demonstrate the ability of the scheme to simulate the practically important solitary wave interaction problem. Throughout this section we consider the initial value problem with periodic boundary conditions.

5.1. **Convergence test and invariants preservation.** Consider the Serre equations (3.1), (3.2) posed in the periodic domain $[-40, 40]$. We solve numerically the initial-periodic boundary value problem with an exact solitary wave solution (2.19) posed as an initial condition. Then, this specific initial disturbance will be translated in space with known celerity under the system dynamics. This particular class of solutions plays an important role in water wave theory and it will allow us to assess the accuracy of the proposed fully discrete scheme (3.5), (3.6). The values of the various physical parameters used in the simulation are given in Table 1.

The error is measured using the discrete L_∞ norm for various successively refined discretizations. The result is shown on Figure 3. Without any surprise, the finite volume scheme (blue line with circles) shows a fairly good second order convergence (with estimated slope ≈ 2.02). For illustrative purposes we show also the error measured for the pseudo-spectral method (red line with crosses) which exhibits an exponential convergence rate.

During all the numerical tests, the mass conservation was satisfied with accuracy of the order $\approx 10^{-14}$. This impressive result is due to excellent local conservative properties of the finite volume method. We also investigate the numerical behaviour of the scheme with respect to the less obvious invariants $\mathcal{H}$ and Q defined in (2.20). These invariants can be computed exactly for solitary waves. However, we do not provide them to avoid cumbersome expressions. For the solitary wave with parameters given in Table 1, the

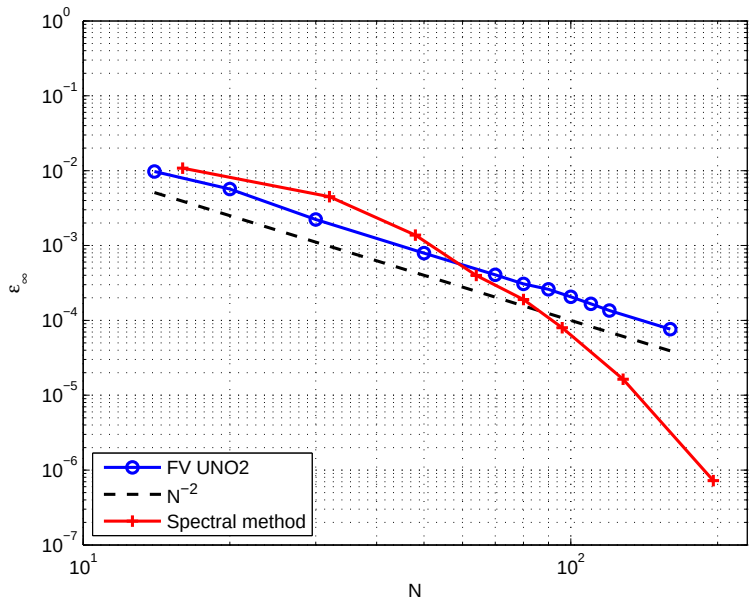

FIGURE 3. Convergence test for the finite volume and spectral methods.

generalized energy and momentum are given by the following expressions:

$$\mathcal{H}_0 = \frac{21\sqrt{7}}{100} + \frac{7\sqrt{3}}{10}\log\frac{\sqrt{21}-1}{\sqrt{21}+1} \approx 0.0178098463,$$
$$Q_0 = \frac{62\sqrt{15}}{225} + \frac{2\sqrt{35}}{5}\log\frac{\sqrt{21}-1}{\sqrt{21}+1} \approx 0.017548002.$$

These values are used to measure the error on these quantities at the end of the simulation. Convergence of this error under the mesh refinement is shown on Figure 4. One can observe a super-convergence phenomenon since apparently we are accurate far beyond the second order that was expected.

5.2. **Solitary wave interaction.** Solitary wave interactions are an important phenomena in nonlinear dispersive waves which have been studied by numerical and analytical methods and results have been compared to experimental evidence. They also often serve as one of the only robust nonlinear benchmark test cases for numerical methods. We mention only a few works among the existing literature. For example, in [34, 41, 14] solitary wave interactions were studied experimentally. The head-on collision of solitary waves was studied in the framework of full Euler equations in [14, 9]. Studies of solitary waves in various approximate models can be found in [32, 18, 2, 20, 19]. To our knowledge, solitary wave collisions for the Serre equations were studied numerically for the first time in the PhD thesis of Seabra-Santos [42]. Finally, there are also a few studies devoted to simulations with full Euler equations [32, 22, 14].

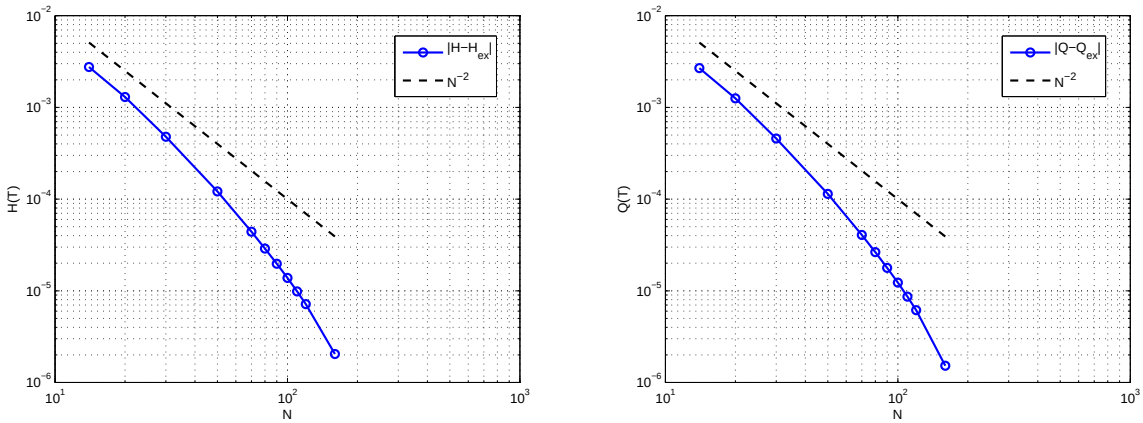

(a) Hamiltonian $\mathcal{H}$ (b) Momentum Q

FIGURE 4. Hamiltonian and generalized momentum conservation convergence of the finite volume method under the mesh refinement measured at the end of the simulation.

First, we study the head-on collision (weak interaction) of two solitary waves of equal amplitude moving in opposite directions. Consider the Serre equations posed in the domain $[-40, 40]$ with periodic boundary conditions. In the present section, we study the head-on collision (weak interaction) of two solitary waves of equal amplitude moving in opposite directions. Initially, two solitary waves of amplitude $a = 0.15$ are located at $x_0 = \pm 20$ (other parameters can be found in Table 1). The computational domain is divided into $N = 1000$ intervals (finite volumes in 1D) of the uniform length $\Delta x = 0.08$. The time step in the fully discrete scheme (3.5), (3.6) is chosen to be $\Delta t \approx 3 \times 10^{-4}$. The process is simulated up to time $T = 36$. The numerical results are presented in Figure 5. As expected, the solitary waves collide quasi-elastically and continue to propagate in opposite directions after the interaction. The value of importance is the maximum amplitude during the interaction process, sometimes referred to as the runup. Usually, it is larger than the sum of the amplitudes of the two initial solitary waves. In this case, we obtain a runup of $0.3130 > 2a = 0.3$.

In order to validate the finite volume simulation, we performed the same computation with the pseudo-spectral method presented briefly in Section 4. We used a fine grid of 1024 nodes and adaptive time stepping. The overall interaction process is visually identical to the finite volume result shown in Figure 5. The runup value according to the spectral method is 0.3127439 showing again the accuracy of our simulation.

The small inelasticity is evident from the small dispersive wave train emerging after the interaction (for an example in a slightly different setting described below, see Figure 14, as first found numerically and experimentally by Seabra-Santos [42].

A second type of solitary wave interaction is the *overtaking collision* (or *strong interaction*) of two solitary waves of different amplitudes moving in the same direction. Sometimes

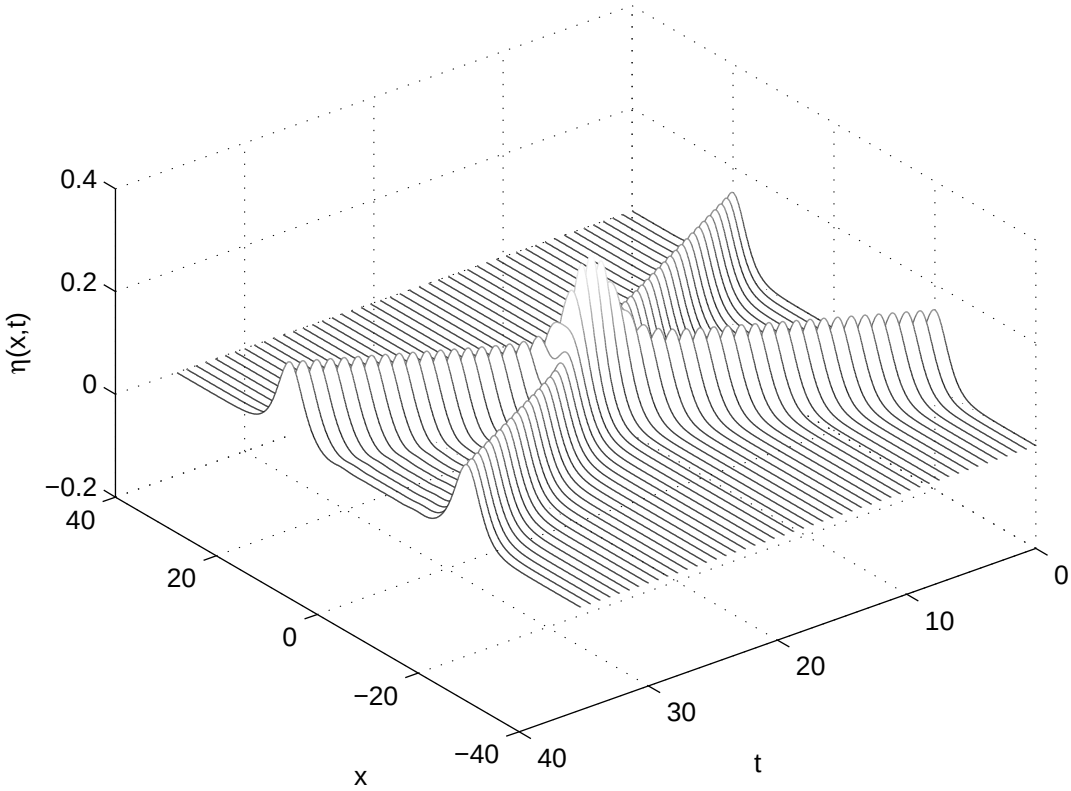

FIGURE 5. Head-on collision of two equal solitary waves simulated with the finite volume scheme.

this situation is also referred to as the following collision or strong interaction. For this case we consider a physical domain $[-75, 75]$ divided into $N = 1000$ equal control volumes.The initial data consists of two separated solitary waves of different amplitudes moving in the same direction. The solitary wave with larger amplitude moves faster and will overtake the smaller wave. This situation was simulated with the finite volume scheme and the numerical results are presented in Figure 6. The parameters used in this simulation are given in Table 2. The strong interaction is also inelastic with a small dispersive tail emerging after the over-taking (Figure 15).

5.3. **Experimental validation.** In this Section we present a comparison between the classical Serre model solved with our finite volume scheme and one head-on collision experiment from [14]. This specific experiment was already considered in the context of Boussinesq-type systems [20].

We simulate a portion of the wave tank $[-0.9, 2.7]$ (divided into $N = 1000$ equal control volumes) where the interaction process takes place. The initial data consists of two solitary

Undisturbed water depth: d	1
Gravity acceleration: g	1
Large solitary wave amplitude: a_1	0.6
Initial position: x_1	-60
Small solitary wave amplitude: a_2	0.1
Initial position: x_2	-45
Final simulation time: T	96
Free parameter: β	1/3

TABLE 2. Values of various parameters used to simulate the overtaking collision.

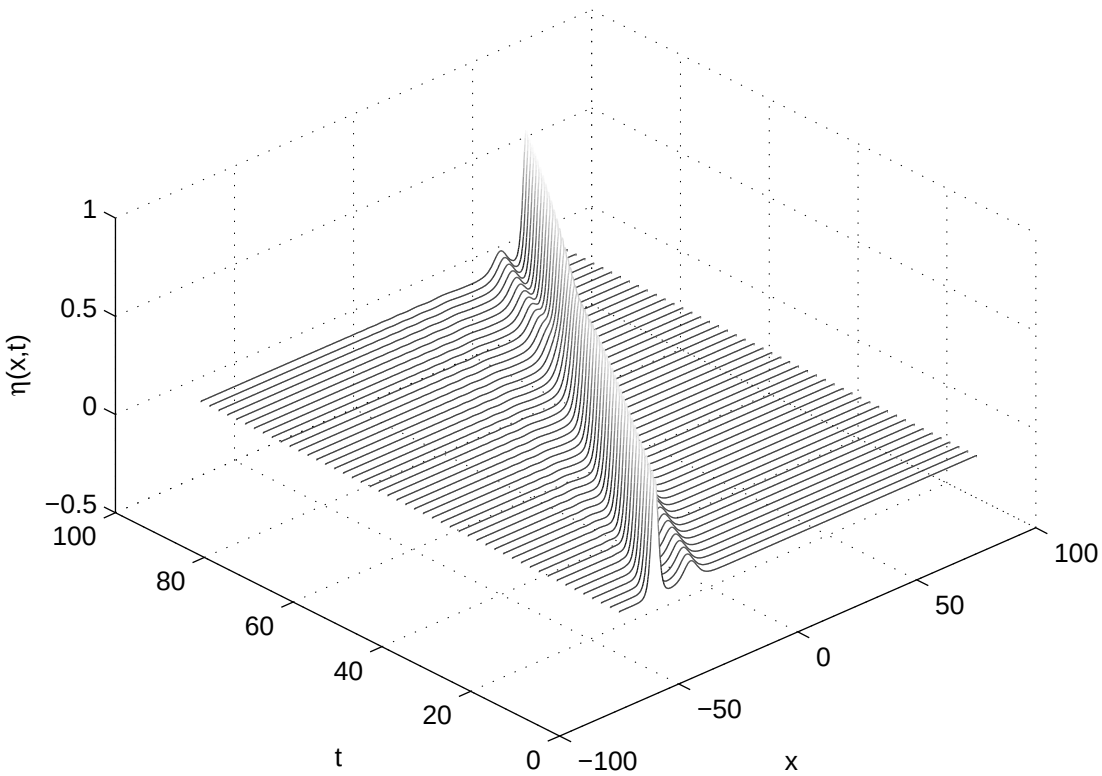

FIGURE 6. Overtaking (or following) collision of two equal solitary waves simulated with the finite volume scheme.

waves (of different amplitudes in this case) moving in opposite directions. The exact parameters are given in Table 3. Simulation snapshots are presented in Figures 7–14. The general agreement is very good validating the Serre equations in water wave theory, along with our numerical developments. Figure 14 shows visible dispersive oscillations

Undisturbed water depth: d [cm]	5
Gravity acceleration: g [m s^{-2}]	9.81
Right-going SW amplitude: a_1 [cm]	1.077
Initial position of the SW-1: x_1 [m]	0.247
Left-going SW amplitude: a_1 [cm]	1.195
Initial position of the SW-2: x_2 [m]	1.348
Final simulation time: T [s]	20.5

TABLE 3. Values of various parameters used to simulate the head-on collision.

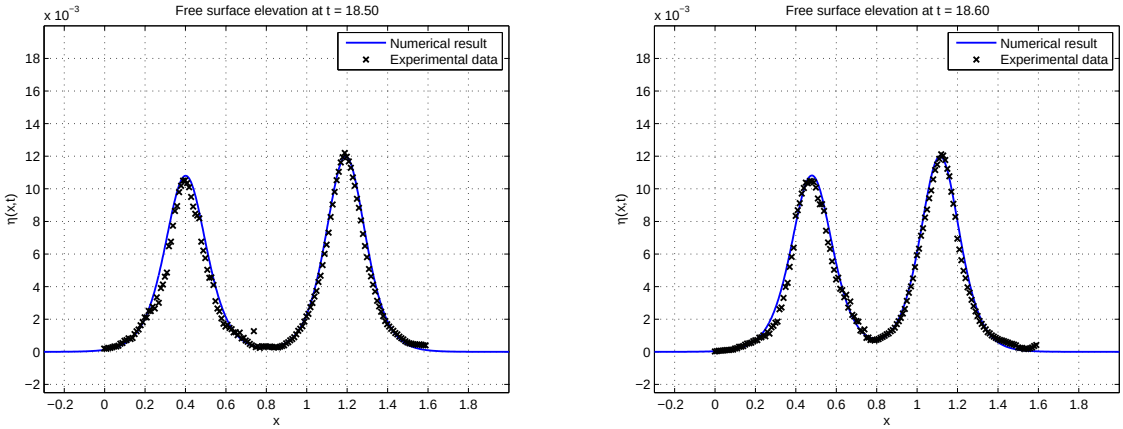

(a) $t = 18.5$ s (b) $t = 18.6$ s

FIGURE 7. Head-on collision of two solitary waves of different amplitudes. Comparison with experimental data.

after the interaction process, numerical evidence of the inelastic character of solitary waves interactions in the framework of the Serre equations.

6. CONCLUSIONS

The current study is devoted to the Serre equations stemming from water wave modeling [44, 7, 16]. First, we presented a derivation of this model using a relaxed variational principle [12]. We then described an Implicit-Explicit finite volume scheme to discretize the equations. The overall theoretical accuracy of the space discretization scheme is of second order accurate. This conclusion is confirmed by comparisons with an exact solitary wave solution. The energy conservation properties of our scheme are also discussed and quantified. In order to validate further our numerical scheme, we present a Fourier-type pseudo-spectral method. Both numerical methods are compared on solitary wave interaction problems. The proposed discretization procedure was successfully validated with several numerical tests along with experimental data. In contrast with the highly accurate

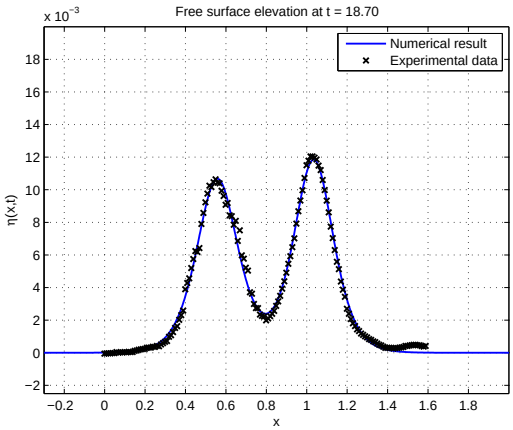

(a) $t = 18.7$ s

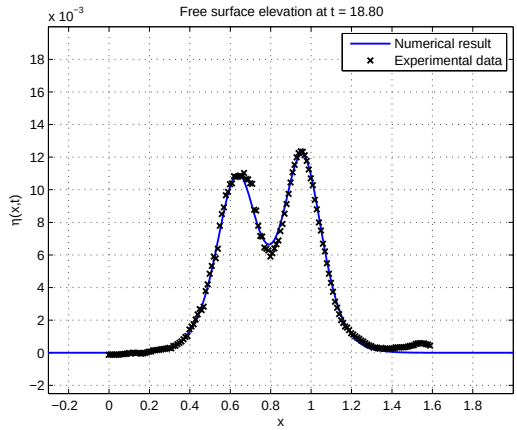

(b) $t = 18.8$ s

FIGURE 8. Head-on collision of two solitary waves of different amplitudes. Comparison with experimental data.

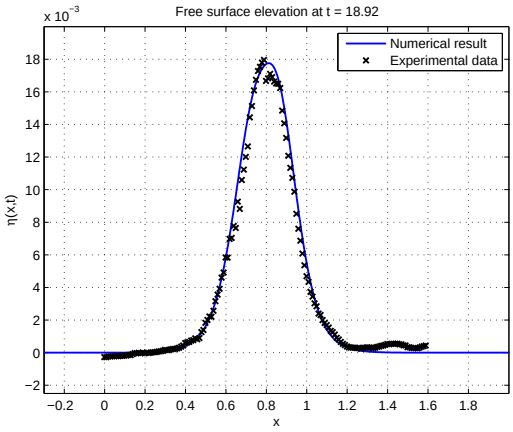

(a) $t = 18.92$ s

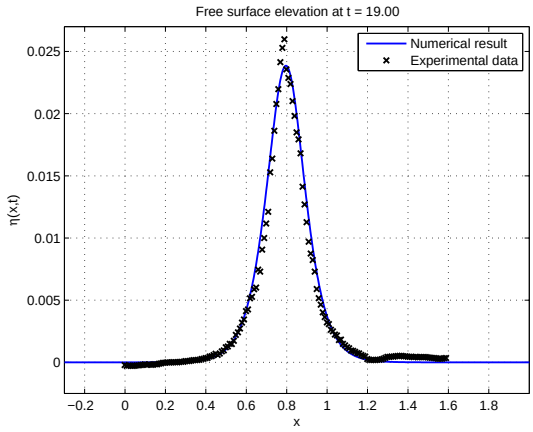

(b) $t = 19.0$ s

FIGURE 9. Head-on collision of two solitary waves of different amplitudes. Comparison with experimental data.

spectral method, the finite volume method has the advantage of being robust and generalizable to realistic complex situations with variable bathymetry, very steep fronts, dry areas, etc. . .

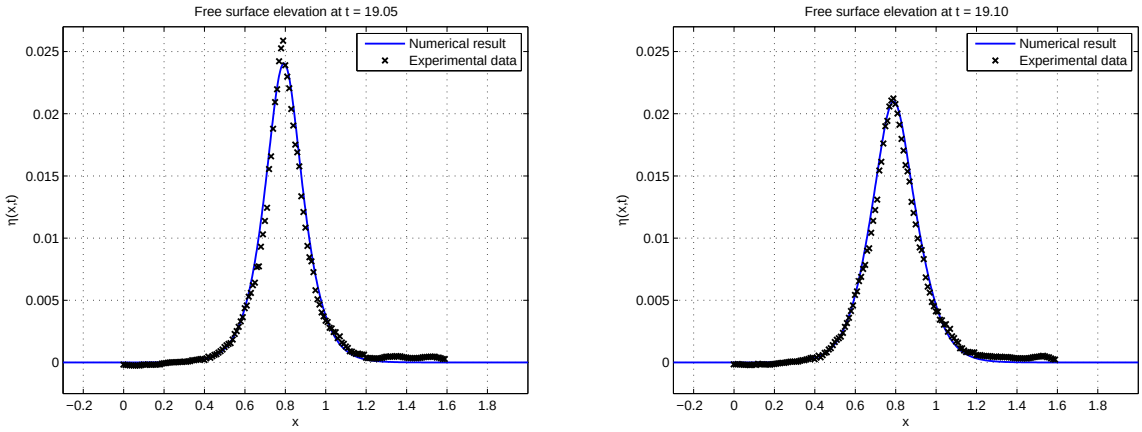

(a) $t = 19.05$ s (b) $t = 19.1$ s

FIGURE 10. Head-on collision of two solitary waves of different amplitudes. Comparison with experimental data.

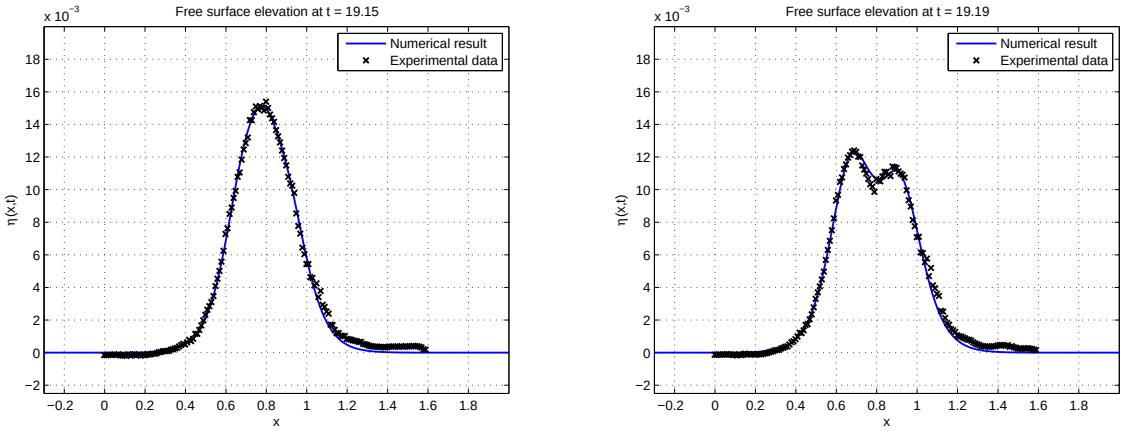

(a) $t = 19.15$ s (b) $t = 19.19$ s

FIGURE 11. Head-on collision of two solitary waves of different amplitudes. Comparison with experimental data.

ACKNOWLEDGEMENTS

D. Dutykh acknowledges the support from French Agence Nationale de la Recherche, project MathOcéan (Grant ANR-08-BLAN-0301-01). P. Milewski acknowledges the support of the University of Savoie which made this joint work possible.

We would like also to thank Brice Eichwald for helpful discussions on spectral methods.

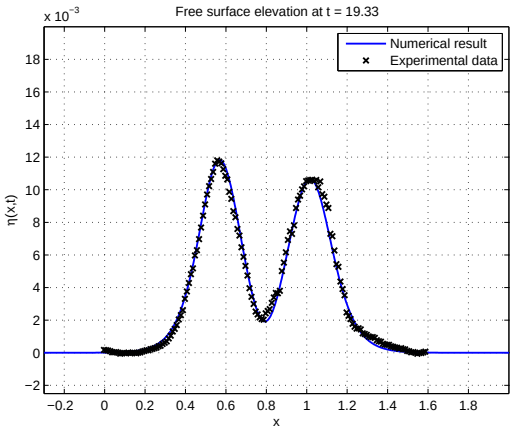

(a) $t = 19.33$ s

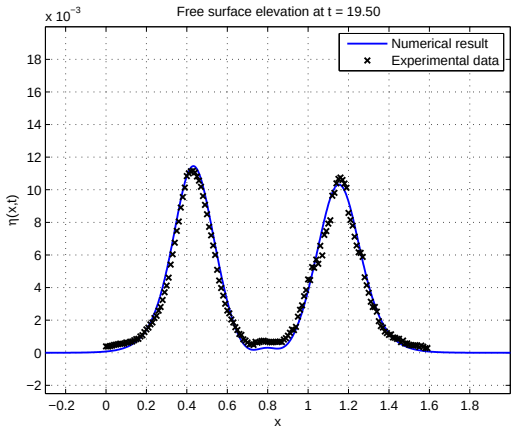

(b) $t = 19.5$ s

FIGURE 12. Head-on collision of two solitary waves of different amplitudes. Comparison with experimental data.

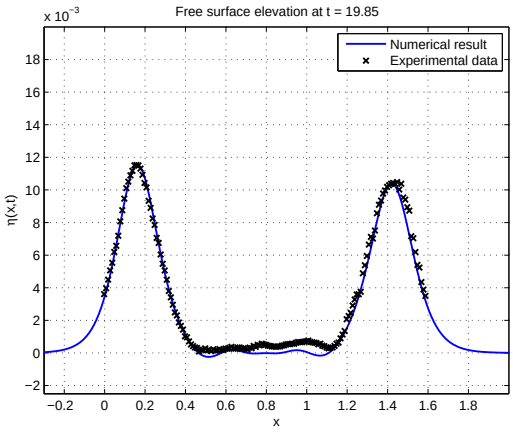

(a) $t = 19.85$ s

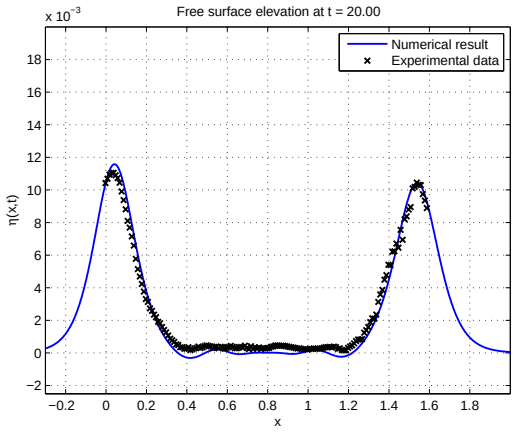

(b) $t = 20.0$ s

FIGURE 13. Head-on collision of two solitary waves of different amplitudes. Comparison with experimental data.

REFERENCES

[1] M. Abramowitz and I. A. Stegun. *Handbook of Mathematical Functions*. Dover, 1965. 6

[2] D. C. Antonopoulos, V. A. Dougalis, and D. E. Mitsotakis. Initial-boundary-value problems for the Bona-Smith family of Boussinesq systems. *Advances in Differential Equations*, 14:27–53, 2009. 14

[3] D. C. Antonopoulos, V. A. Dougalis, and D. E. Mitsotakis. Numerical solution of Boussinesq systems of the Bona-Smith family. *Appl. Numer. Math.*, 30:314–336, 2010. 2

[4] P. Avilez-Valente and F.J. Seabra-Santos. A high-order Petrov-Galerkin finite element method for the classical Boussinesq wave model. *Int. J. Numer. Meth. Fluids*, 59:969–1010, 2009. 2

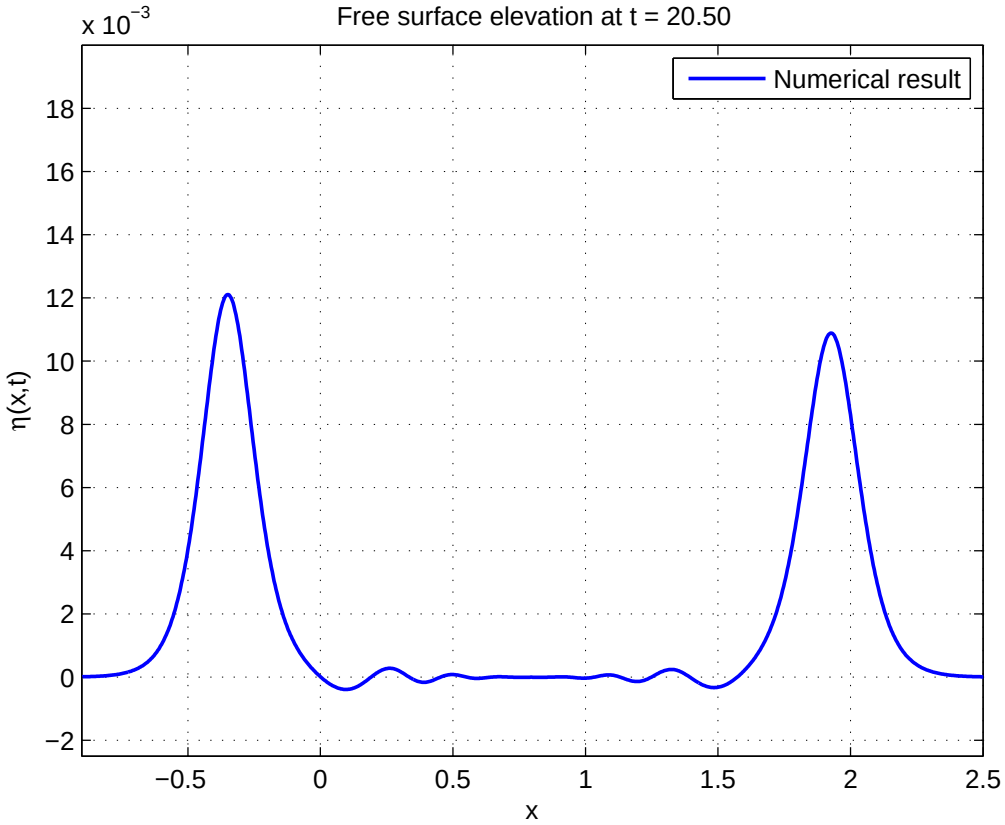

FIGURE 14. Dispersive tail after head-on collision of two solitary waves (weak interaction).

[5] T.J. Barth. Aspects of unstructured grids and finite-volume solvers for the Euler and Navier-Stokes equations. *Lecture series - van Karman Institute for Fluid Dynamics*, 5:1–140, 1994. 7, 10

[6] T.J. Barth and M. Ohlberger. *Encyclopedia of Computational Mechanics, Volume 1, Fundamentals*, chapter Finite Volume Methods: Foundation and Analysis. John Wiley and Sons, Ltd, 2004. 7, 10

[7] E. Barthélémy. Nonlinear shallow water theories for coastal waves. *Surveys in Geophysics*, 25:315–337, 2004. 2, 18

[8] T.B. Benjamin and P. Olver. Hamiltonian structure, symmetries and conservation laws for water waves. *J. Fluid Mech*, 125:137–185, 1982. 5

[9] J. Chambarel, C Kharif, and J. Touboul. Head-on collision of two solitary waves and residual falling jet formation. *Nonlin. Processes Geophys.*, 16:111–122, 2009. 14

[10] R. Cienfuegos, E. Barthelemy, and P. Bonneton. A fourth-order compact finite volume scheme for fully nonlinear and weakly dispersive Boussinesq-type equations. Part I: Model development and analysis. *Int. J. Numer. Meth. Fluids*, 51:1217–1253, 2006. 2

[11] R. Cienfuegos, E. Barthelemy, and P. Bonneton. A fourth-order compact finite volume scheme for fully nonlinear and weakly dispersive Boussinesq-type equations. Part II: Boundary conditions and model validation. *Int. J. Numer. Meth. Fluids*, 53:1423–1455, 2007. 2

[12] D. Clamond and D. Dutykh. Practical use of variational principles for modeling water waves. *Submitted*, `http://arxiv.org/abs/1002.3019/`, 2011. 4, 5, 18

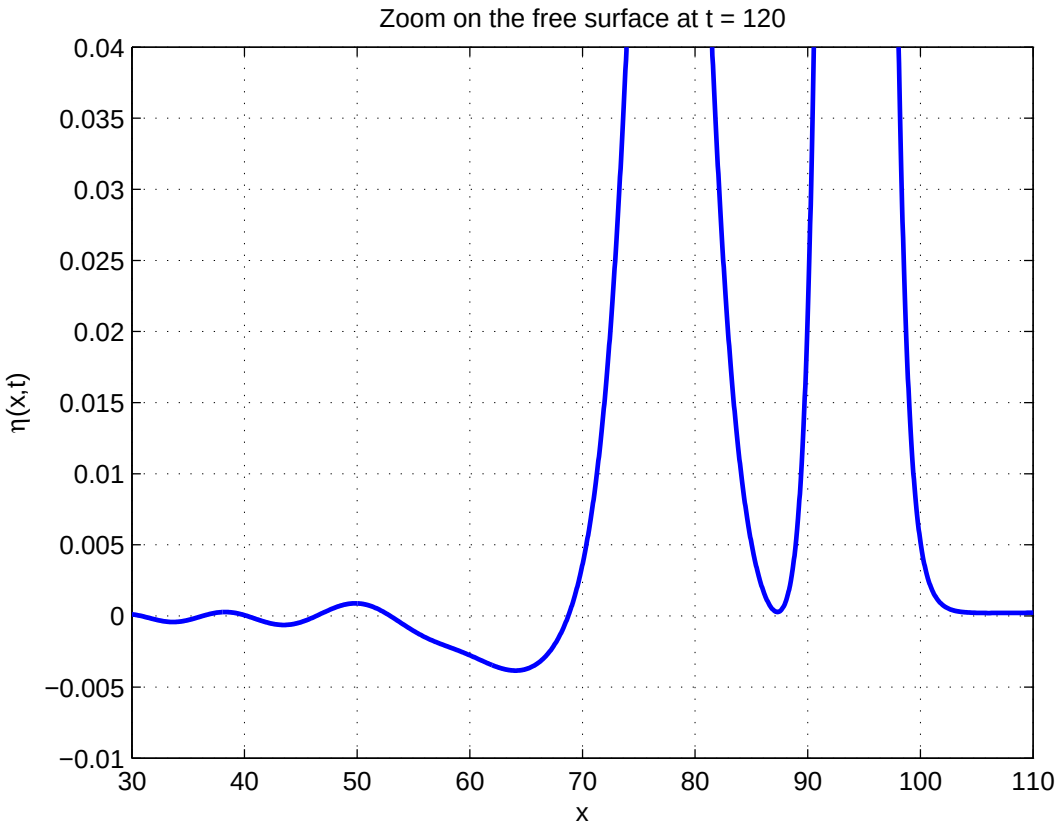

FIGURE 15. Dispersive tail after overtaking collision of two solitary waves (strong interaction).

[13] D. Clamond and J. Grue. A fast method for fully nonlinear water-wave computations. *J. Fluid. Mech.*, 447:337–355, 2001. 12

[14] W. Craig, P. Guyenne, J. Hammack, D. Henderson, and C. Sulem. Solitary water wave interactions. *Phys. Fluids*, 18:57–106, 2006. 14, 16

[15] A.D.D. Craik. The origins of water wave theory. *Ann. Rev. Fluid Mech.*, 36:1–28, 2004. 1

[16] F. Dias and P. Milewski. On the fully-nonlinear shallow-water generalized Serre equations. *Physics Letters A*, 374(8):1049–1053, 2010. 2, 18

[17] V. A. Dougalis and D. E. Mitsotakis. Theory and numerical analysis of Boussinesq systems: A review. In N. A. Kampanis, V. A. Dougalis, and J. A. Ekaterinaris, editors, *Effective Computational Methods in Wave Propagation*, pages 63–110. CRC Press, 2008. 2

[18] V.A. Dougalis and D.E. Mitsotakis. *Advances in scattering theory and biomedical engineering*, chapter Solitary waves of the Bona-Smith system, pages 286–294. World Scientific, New Jersey, 2004. 14

[19] D. Dutykh, Th. Katsaounis, and D. Mitsotakis. Finite volume methods for unidirectional dispersive wave models. *Submitted*, `http://hal.archives-ouvertes.fr/hal-00538043/`, 2010. 2, 14

[20] D. Dutykh, Th. Katsaounis, and D. Mitsotakis. Finite volume schemes for dispersive wave propagation and runup. *Journal of Computational Physics*, 230:3035–3061, 2011. 2, 9, 10, 14, 16

[21] W.F. Ford and A. Sidi. An algorithm for a generalization of the Richardson extrapolation process. *SIAM Journal on Numerical Analysis*, 24(5):1212–1232, 1987. 11

[22] D. Fructus, D. Clamond, O. Kristiansen, and J. Grue. An efficient model for threedimensional surface wave simulations. Part i: Free space problems. *J. Comput. Phys.*, 205:665–685, 2005. 12, 14

[23] J.-M. Ghidaglia, A. Kumbaro, and G. Le Coq. Une méthode volumes-finis à flux caractéristiques pour la résolution numérique des systèmes hyperboliques de lois de conservation. *C. R. Acad. Sci. I*, 322:981–988, 1996. 8

[24] J.-M. Ghidaglia, A. Kumbaro, and G. Le Coq. On the numerical solution to two fluid models via cell centered finite volume method. *Eur. J. Mech. B/Fluids*, 20:841–867, 2001. 8

[25] A. E. Green, N. Laws, and P. M. Naghdi. On the theory of water waves. *Proc. R. Soc. Lond. A*, 338:43–55, 1974. 2

[26] A. Harten. ENO schemes with subcell resolution. *J. Comput. Phys*, 83:148–184, 1989. 9

[27] A. Harten and S. Osher. Uniformly high-order accurate nonscillatory schemes, I. *SIAM J. Numer. Anal.*, 24:279–309, 1987. 9

[28] J.W. Kim, K.J. Bai, R.C. Ertekin, and W.C. Webster. A derivation of the Green-Naghdi equations for irrotational flows. *Journal of Engineering Mathematics*, 40(1):17–42, 2001. 5

[29] N.E. Kolgan. Finite-difference schemes for computation of three dimensional solutions of gas dynamics and calculation of a flow over a body under an angle of attack. *Uchenye Zapiski TsaGI [Sci. Notes Central Inst. Aerodyn]*, 6(2):1–6, 1975. 9

[30] H. Lamb. *Hydrodynamics*. Cambridge University Press, 1932. 3

[31] Y.A. Li. Hamiltonian structure and linear stability of solitary waves of the Green-Naghdi equations. *J. Nonlin. Math. Phys.*, 9, 1:99–105, 2002. 6, 7

[32] Y.A. Li, J.M. Hyman, and W. Choi. A numerical study of the exact evolution equations for surface waves in water of finite depth. *Stud. Appl. Maths.*, 113:303–324, 2004. 14

[33] J.C. Luke. A variational principle for a fluid with a free surface. *J. Fluid Mech.*, 27:375–397, 1967. 3

[34] T. Maxworthy. Experiments on collisions between solitary waves. *J Fluid Mech*, 76:177–185, 1976. 14

[35] C.C. Mei. *The applied dynamics of ocean surface waves*. World Scientific, 1994. 3

[36] J.W. Miles and R. Salmon. Weakly dispersive nonlinear gravity waves. *J. Fluid Mech.*, 157:519–531, 1985. 5

[37] P. Milewski and E. Tabak. A pseudospectral procedure for the solution of nonlinear wave equations with examples from free-surface flows. *SIAM J. Sci. Comput.*, 21(3):1102–1114, 1999. 12

[38] S.M. Mirie and C.H. Su. Collision between two solitary waves. Part 2. A numerical study. *J. Fluid Mech*, 115:475–492, 1982. 2

[39] D.E. Mitsotakis. Boussinesq systems in two space dimensions over a variable bottom for the generation and propagation of tsunami waves. *Math. Comp. Simul.*, 80:860–873, 2009. 2

[40] A.A. Petrov. Variational statement of the problem of liquid motion in a container of finite dimensions. *PMM*, 28(4):917–922, 1964. 3

[41] D.P. Renouard, F.J. Seabra-Santos, and A.M. Temperville. Experimental study of the generation, damping, and reflexion of a solitary wave. *Dynamics of Atmospheres and Oceans*, 9(4):341–358, 1985. 14

[42] F.J. Seabra-Santos. *Contribution à l'étude des ondes de gravité bidimensionnelles en eau peu profonde*. PhD thesis, Institut National Polytechnique de Grenoble, 1985. 14, 15

[43] F.J. Seabra-Santos, D.P. Renouard, and A.M. Temperville. Numerical and experimental study of the transformation of a solitary wave over a shelf or isolated obstacle. *J. Fluid Mech*, 176:117–134, 1987. 2

[44] F. Serre. Contribution à l'étude des écoulements permanents et variables dans les canaux. *La Houille blanche*, 8:374–388 & 830–872, 1953. 2, 5, 18

[45] G. Söderlind. Digital filters in adaptive time-stepping. *ACM Trans. Math. Software*, 29:1–26, 2003. 13

[46] G. Söderlind and L. Wang. Adaptive time-stepping and computational stability. *Journal of Computational and Applied Mathematics*, 185(2):225–243, 2006. 13

[47] J.J. Stoker. *Water waves, the mathematical theory with applications*. Wiley, 1958. 3

[48] C.H. Su and C.S. Gardner. Korteweg-de Vries equation and generalizations. III. Derivation of the Korteweg-de Vries equation and Burgers equation. *J. Math. Phys.*, 10:536–539, 1969. 2
[49] Lloyd N. Trefethen. *Spectral methods in MatLab*. Society for Industrial and Applied Mathematics, Philadelphia, PA, USA, 2000. 12
[50] B. van Leer. Towards the ultimate conservative difference scheme V: a second order sequel to Godunov' method. *J. Comput. Phys.*, 32:101–136, 1979. 9
[51] B. van Leer. Upwind and high-resolution methods for compressible flow: From donor cell to residual-distribution schemes. *Communications in Computational Physics*, 1:192–206, 2006. 9
[52] J.H. Verner. Explicit Runge–Kutta methods with estimates of the local truncation error. *SIAM J. Num. Anal.*, 15(4):772–790, 1978. 12
[53] G. B. Whitham. A general approach to linear and non-linear dispersive waves using a Lagrangian. *J. Fluid Mech.*, 22:273–283, 1965. 3
[54] G.B. Whitham. *Linear and nonlinear waves*. John Wiley & Sons Inc., New York, 1999. 3
[55] Y. Xing and C.-W. Shu. High order finite difference weno schemes with the exact conservation property for the shallow water equations. *J. Comput. Phys.*, 208:206–227, 2005. 9
[56] V.E. Zakharov. Stability of periodic waves of finite amplitude on the surface of a deep fluid. *J. Appl. Mech. Tech. Phys.*, 9:1990–1994, 1968. 3

LAMA, UMR 5127 CNRS, Université de Savoie, Campus Scientifique, 73376 Le Bourget-du-Lac Cedex, France
E-mail address: `Denys.Dutykh@univ-savoie.fr`
URL: `http://www.lama.univ-savoie.fr/~dutykh/`

Laboratoire J.-A. Dieudonné, Université de Nice – Sophia Antipolis, Parc Valrose, 06108 Nice cedex 2, France
E-mail address: `diderc@unice.fr`
URL: `http://math.unice.fr/~didierc/`

University of Wisconsin, Dept. of Mathematics, 480 Lincoln Dr. Madison, WI 53706, USA
E-mail address: `milewski@math.wisc.edu`
URL: `http://www.math.wisc.edu/~milewski/`

IMA, University of Minnesota, 114 Lind Hall and 207 Church Street SE, Minneapolis MN 55455, USA
E-mail address: `dmitsot@gmail.com`
URL: `http://sites.google.com/site/dmitsot/`